

Tuning nanoscale adhesive contact behavior to a near ideal Hertzian state via graphene coverage

Yongchao Chen¹, Zhizi Guan¹, Yongtao Yao², Hailong Wang^{1,*}

¹ CAS Key Laboratory of Mechanical Behavior and Design of Materials, Department of Modern Mechanics, University of Science and Technology of China, Hefei 230027, China

² National Key Laboratory of Science and Technology on Advanced Composites in Special Environments, Harbin Institute of Technology, Harbin, Heilongjiang 150080, China

*e-mail: hailwang@ustc.edu.cn

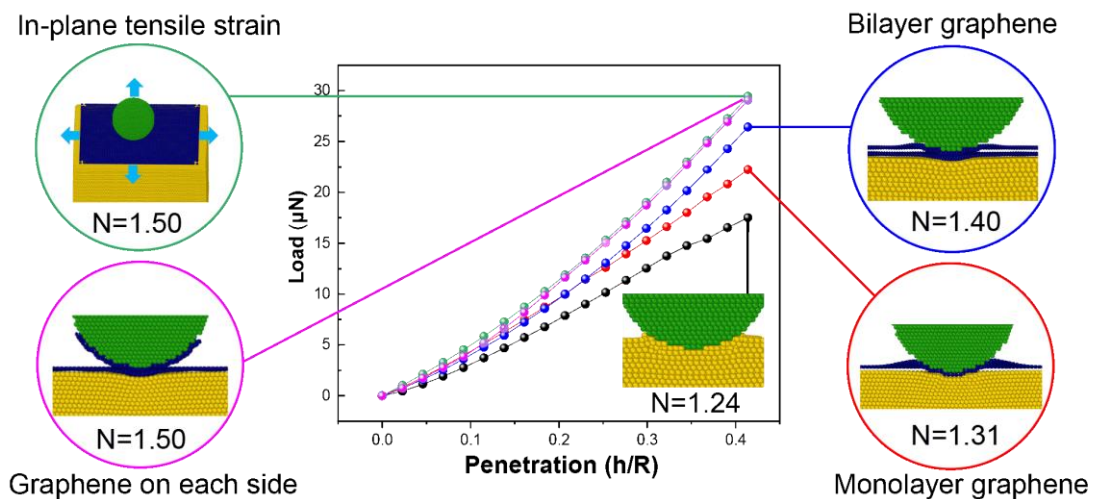
Highlights

- Graphene coatings can tune elastic contact behavior of substrate into a near ideal Hertzian state through adhesion elimination.
- Contact tuning is more significant by using multilayer graphene, coating on both tip and substrate, or applying in-plane strain.
- Large size indenters get less influence from adhesion due to confinement of adhesion range between tip and substrate.

ABSTRACT

We carry out molecular statics (MS) simulations to study the indentation process of Pt (111) surfaces with indenter radius from 5 to 20 nm. The substrate and indenter surfaces are either bare or graphene-covered. Our simulations show that the influences of adhesion between bare substrate and indenter tip can be significantly reduced by

decreasing the adhesion strength and adhesion range between atoms on substrate and indenter, or enhancing the substrate stiffness. Our results suggest that the elastic response of substrate exhibits less adhesion by coating graphene layers on either side of the contacting interface, which is attributed to the weak interaction between graphene layers. Based on these principles obtained for bare substrate, the nanoscale contact behavior of substrate can be tuned into a near-ideal Hertzian state by increasing the number of graphene layers, applying pre-strains to graphene on substrate, or using large size indenters. Our research provides a theoretical guidance for designing adhesion-less coatings for the AFM probes and MEMS/NEMS systems.



Keywords

Adhesive contact; Hertzian contact theory; Multilayer graphene-coating; In-plane straining; Size effect; Molecular statics simulation

1. Introduction

Graphene (Gr), a two dimensional (2D) material made of a single layer of carbon atoms [1], possesses several exotic properties, which make it uniquely suited as a protective coating and superior lubricant for electrical contacts [2, 3]: ultimate tensile strength of 130 GPa [4], ultralow surface energy 46.7 mJ/m² [5, 6], and atomically-thin layer [7]. As a result, remarkable achievements have been made in exploring the significant low-friction and anti-wear properties of graphene, such as layer-dependent transient friction strengthening [8], friction tuning via in-pane straining [9], and nanowear reduction by suppressing the contact pressure fluctuation [10]. Apart from graphene effects in lubrication, molecular dynamics (MD) simulations of nanoindentation show that graphene coating can make metallic substrate more resistant to plastic deformation and essentially improve the load-bearing capacity, which is attributed to atomic-scale surface roughness smoothing [11, 12], homogenization of contact stress distribution beneath tip [13] and interactions between dislocations and graphene coating interface [14].

Most of the studies on friction and nanoindentation focused on the lateral friction behaviors [8, 9, 15, 16] and plastic deformation [11-13] but ignored the detailed behaviors during initial elastic contact stage. Nevertheless, in fact, elastic contact is not only an inevitable process prior to friction and plastic stage, but also a completely different state for graphene protective mechanism. Recently, it is reported that the experimental elastic load-displacement curves from sub-nanometer indentation on graphene-coated Cu film are in a closer agreement with the Hertz model compared to

bare Cu [17, 18]. Meanwhile, MD simulations have also revealed that graphene regularizes the response between indenter tip and substrate and yields a Hertz-type contact (with the modulus of the bulk substrate) owing to the elimination of interatomic adhesion [11, 18]. Simultaneously, tremendous interests have been invested into the studies of the adhesive contact behavior between various materials, such as the theoretical description of adhesive contact [19, 20], material transfer due to adhesion [21] and different influential factors for adhesion strength [22, 23]. Hence, a well-established theory of this graphene modifying phenomenon will open a new route for the research on adhesive contact. However, many influence factors on this regulating effect, such as the number of graphene layers, in-plane pre-strain in graphene, and the size of indenter, are generally neglected, which all have possibilities to exert significant effects on the elastic response to nanoscale adhesive contact. With regard to the importance of surface adhesion and the contact behavior of graphene coated surfaces, a better insight into graphene's adhesion and contact properties is highly required.

In this work, through molecular statics (MS) simulations, we show that the elastic contact behavior of metallic substrate exhibits a higher load bearing capacity as well as a near ideal Hertzian contact, which can be achieved by coating graphene on either side of the contact interface (upper spherical or lower flat surfaces). We analyze the atomic-scale microstructure in the contact region between the tip and bare substrate, and find that the adhesion can be mitigated by reducing the adhesion strength and adhesion range of interaction between atoms on tip and substrate, or enhancing the stiffness of substrate surface. More specifically, the adhesion between tip and graphene-coated substrate can

be significantly reduced by increasing covered graphene layers or applying pre-strains to graphene monolayer, which further regulates the elastic response and yields a Hertz-type contact. Moreover, the regulation of elastic contact behavior of graphene-coated substrate can be enhanced by increasing the indenter size due to the reduction of relative adhesive area on the indenter, especially when high adhesion occurs between tip and substrate. As demonstrated in previous studies [11, 12, 17, 18, 24, 25], this adhesion-less contact behavior regulated by graphene layers makes it possible to measure elastic modulus of various substrate materials via fitting the load-displacement curves extracted from nanoindentation into Hertz theory. Aside from fundamental interests, proper tribological engineering that takes adhesion into account is crucial in developing reliable MEMS devices such as the digital mirror device and MEMS switches [26, 27], in which cases the transfer between contact and materials is generally a big issue. Hence, our investigation provides a theoretical guidance for designing adhesion-less coatings for the AFM probes and MEMS/NEMS systems [28].

2. Methods

MS simulations in LAMMPS [29] are carried out to model the nanoindentation process on a Pt substrate with a rigid semispherical Pt tip. The tips are moved in steps of 0.05\AA , after which the systems are relaxed to the next local minimum until atomic forces drop below 10^{-4} eV/\AA . To eliminate the influence of atomic-scale geometry, tips are produced by displacing atoms of a (111) face-centered cubic (fcc) slab normal to the slab surface such that surface atoms precisely follow the surface of a sphere [11]. The radii of bare or graphene-layers-wrapped tips are varied from 5 to 20 nm to study size

effects. Substrates are also bare or coated with graphene layers, periodically repeated cubic Pt crystals in their face centered cubic (fcc) ground-state structure with (111) surfaces exposed towards the indenter. Graphene layers are placed on the surfaces with its $\langle 10 \rangle$ direction parallel to the Pt $\langle 110 \rangle$ direction. One layer of atoms at the bottom of the surface is fixed during the calculations to anchor the solid within the simulation cell. To minimize the influence of periodic indenter images, the side length and height of the substrate is chosen to be roughly five and two times the indenter radius, respectively.

The embedded atom method (EAM) potential [30] is used to model the Pt-Pt interaction within the substrate. The C-C interaction within the same graphene sheet is modeled using the second-generation empirical reactive bond-order (REBO2) potential [31] with a modified cutoff scheme [32]. To study the effect of substrate stiffness, the Tersoff [33] and EAM [34] potential are applied for Si and Al substrate, respectively. The truncated Lennard-Jones (LJ) potential is used for the atomic interactions among tip, graphene, and substrate,

$$U(r) = \begin{cases} 4\varepsilon \left(\left(\frac{\sigma}{r} \right)^{12} - \left(\frac{\sigma}{r} \right)^6 \right) - 4\varepsilon \left(\left(\frac{\sigma}{r_c} \right)^{12} - \left(\frac{\sigma}{r_c} \right)^6 \right), & r < r_c \\ 0, & r \geq r_c \end{cases} \quad (1)$$

where the parameters are $\varepsilon_{Pt-Pt} = 0.0683 \text{ eV}$ and $\sigma_{Pt-Pt} = 0.254 \text{ nm}$ for the Pt-Pt interaction between tip and substrate, $\varepsilon_{Pt-C} = 0.0112 \text{ eV}$ and $\sigma_{Pt-C} = 0.297 \text{ nm}$ for the Pt-C interaction between tip and graphene, $\varepsilon_{C-C} = 0.00284 \text{ eV}$ and $\sigma_{C-C} = 0.34 \text{ nm}$ for the C-C interaction in different graphene layers, and $r_c = 2.5\sigma$ as the cutoff radius [35]. To investigate the effects of adhesion strength and adhesion range

on nanoscale contact behavior, we tune the depth of the potential well (ε) and the equilibrium distance ($\sigma_0 = 2^{1/6}\sigma$). For convenience sake, the subscript *TS*, *GT*, *GS* denotes the interaction for tip/substrate, graphene/tip, and graphene/substrate, respectively. For bare substrate, we set $\varepsilon_{TS} = 0.5\varepsilon_{Pt-Pt}$ and $\varepsilon_{TS} = 2\varepsilon_{Pt-Pt}$ for strong and weak adhesion, $\sigma_{TS} = 0.5\sigma_{Pt-Pt}$ and $\sigma_{TS} = 2\sigma_{Pt-Pt}$ for short-range and long-range adhesion. For graphene-coated substrate, to optimally model extreme conditions, we artificially enlarge the depth of the potential well $\varepsilon_{GT} = 10\varepsilon_{Pt-C}$, or $\varepsilon_{GS} = 10\varepsilon_{Pt-C}$ for strong adhesion. Therefore, 4 typical adhesion cases are considered for nanoindentation on graphene-covered substrate in this work, , namely, Normal Adhesion ($\varepsilon_{GS} = \varepsilon_{C-Pt}, \varepsilon_{GT} = \varepsilon_{C-Pt}$), Strong Gr-sub ($\varepsilon_{GS} = 10\varepsilon_{C-Pt}, \varepsilon_{GT} = \varepsilon_{C-Pt}$), Strong Gr-tip ($\varepsilon_{GS} = \varepsilon_{C-Pt}, \varepsilon_{GT} = 10\varepsilon_{C-Pt}$), and Strong Adhesion ($\varepsilon_{GS} = 10\varepsilon_{C-Pt}, \varepsilon_{GT} = 10\varepsilon_{C-Pt}$).

3. Results and Discussion

3.1. Influential factors for nanoscale adhesive contact on bare substrate

We start with indenting the bare substrate and analyzing the force versus displacement curves from these simulations to study the effects of tip-substrate adhesion and substrate stiffness on contact behavior. In this regard, Hertz theory predicts that the force P due to a displacement h on a sphere of radius R is given by,

$$P = (4E^*R^2/3) (h/R)^{3/2} \quad (2)$$

where the contact modulus $E^* = E/(1 - \nu^2)$ for a rigid and isotropic substrate. To quantify the deviation from the Hertz prediction, the exponent N of a specific contact

behavior is identified by fitting $P = (4E^*R^2/3) (h/R)^N$ extracted from the load-displacement curve. Fig. 1 summarizes the plots of force P on the indenter as a function of scaled penetration depth h/R obtained for indenter radius of $R = 5nm$ on bare substrate. Fig. 1a shows that, in the elastic regime, the purely repulsive contact behavior is highly consistent to Hertz theory with a fitting exponent $N = 1.48$ (red curve). In Fig. 1a, the negligible deviation to the Hertz prediction ($N = 1.50$ for dashed line) is due to the morphological difference from a diamond tip to a strict round tip. For comparison, the force-displacement curve is also plotted for the normal tip-substrate adhesion in all panels ($N = 1.25$ for black curves), in which the deviation from Hertz theory is apparent due to the attractive contribution of Lenard-Jones potential. This result indicates that with a purely repulsive interaction, nanoindentation can follow Hertz theoretical prediction even if graphene is absent.

To further investigate the effect of adhesion between tip and substrate, we systemically tune the adhesion strength and range of atomic interaction as well as substrate stiffness to compare with the normal case. Fig. 1b shows that compared with normal case ($N = 1.25$ for black curve), weak adhesion ($\varepsilon_{TS} = 0.5\varepsilon_{Pt-Pt}$) leads to a smaller deviation ($N = 1.45$ for red curve) from the Hertz prediction. Furthermore, force fluctuation (blue circle in Fig. 1b) can be aroused owing to the instant adhesion of Pt atoms to the tip when the adhesive force is strong enough. The inset of Fig. 1b clearly shows atoms transferring to the tip during the contact process, which does not appear in the snapshot for the normal case (inset, Fig. 1a). The influence of equilibrium distance is illuminated

in Fig.1c that a short-range adhesive interaction ($\sigma_{TS} = 0.5\sigma_{Pt-Pt}$) can surely cause less deviations ($N = 1.40$ for red curve) on contact forces.

From the inset of Fig. 1c, we can detect the specific distribution of atomic stress σ_{zz} , in which only the atoms of outer sphere and near contact region are affected by apparent adhesive forces (red colored). It is clear that this phenomenon is caused by restrictions from force range between indenter and substrate. And we also note that the large force drop in some curves in Fig. 1 indicates plastic deformation in the substrate. Additional MS simulations are performed to compare adhesive contact behaviors for substrates with various stiffness values E^* . Here, we change the substrate materials respectively into Si ($E_{Si}^* = 320GP$) and Al ($E_{Al}^* = 70GPa$). Fig. 1d illustrates that a stiffer substrate suffers less deviation from adhesion and has a contact behavior closer to Hertz prediction ($N = 1.37$ for red curve). This can be explained as atoms at the contact area will be strongly constrained by atoms around and cannot adhere to the tip. As a result, hypothesis that adhesion can impose the deviation to ideal Hertz contact behavior can be corroborated and more specifically, this deviation has two main characteristics, i.e., a lower component N and more force fluctuation.

Therefore, there are three main factors affecting the adhesion, i.e., adhesion strength, adhesion range, and substrate stiffness, serving as an efficient guidance for adhesion mitigation. The following intuitive question is on how to minimize or even eliminate adhesion effects during nanoindentation.

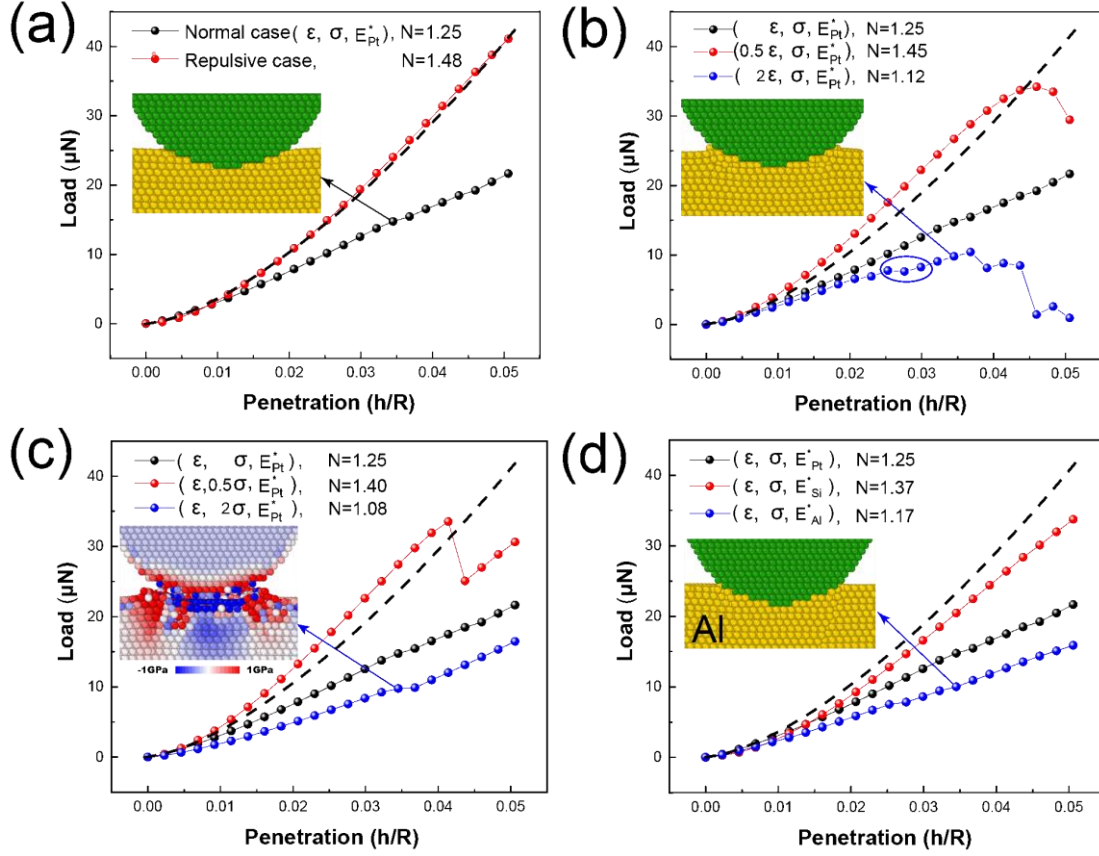


Figure 1. Factors that influence nanoscale adhesive contact on bare substrate. (a) A near-ideal Hertz contact behavior when employing a purely repulsive interaction, compared with a normal interaction case ($\epsilon_{TS} = \epsilon_{Pt-Pt}, \sigma_{TS} = \sigma_{Pt-Pt}, E^* = E_{Pt}^*$). (b-d) The effects of (b) adhesion strength ($\epsilon_{TS} = 0.5\epsilon_{Pt-Pt}, \epsilon_{Pt-Pt}, 2\epsilon_{Pt-Pt}$), (c) adhesion range ($\sigma_{TS} = 0.5\sigma_{Pt-Pt}, \sigma_{Pt-Pt}, 2\sigma_{Pt-Pt}$), and (d) substrate stiffness ($E^* = E_{Al}^*, E_{Pt}^*, E_{Si}^*$) on the degree of deviations from the Hertz prediction. Plots of force P vs. scaled penetration depth h/R for indenter radii of $R = 5nm$ are depicted in each subfigure. (insets) The snapshots (green for tip atoms and yellow for substrate atoms) indicate the stronger deviations for (b) strong adhesion strength ($\epsilon_{TS} = 2\epsilon_{Pt-Pt}$), (c) long adhesion range ($\sigma_{TS} = 2\sigma_{Pt-Pt}$), and (d) soft substrate ($E^* = E_{Al}^*$) are contributed to more substrate atoms transferring to the tips. The inset in (c) illustrates the stress

distribution during contact as well, where the color of each atom represents the atomic stress σ_{zz} component. For consistency, the color scheme for the atomic plots is preserved in the remaining figures. The indenter radius of $R = 5\text{nm}$ is maintained in all the atomic simulations if not mentioned.

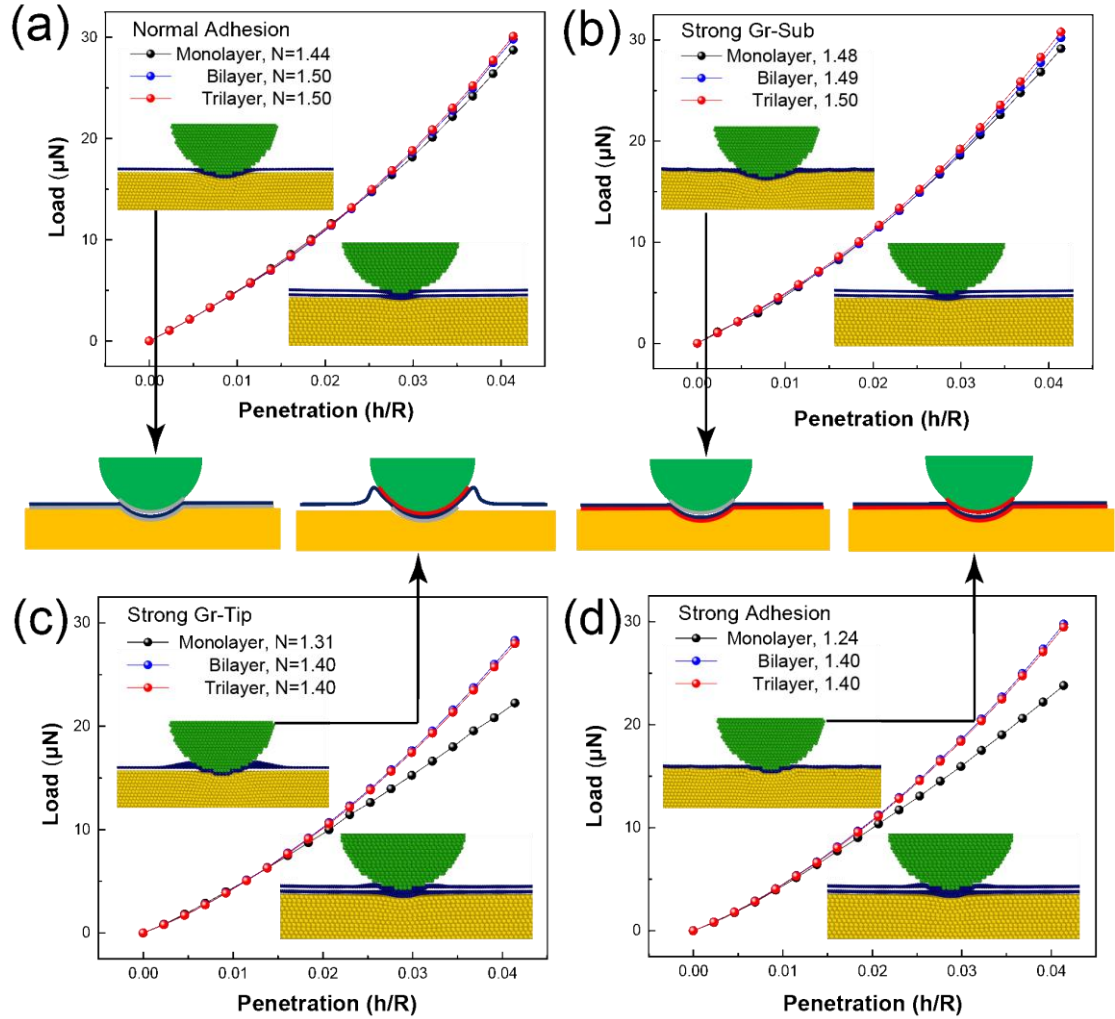


Figure 2. The influence of layer number of graphene coatings on degree of deviations from the Hertz prediction for typical interactions between tips, graphene layers, and substrates: (a) Normal Adhesion ($\epsilon_{GS} = \epsilon_{C-Pt}$, $\epsilon_{GT} = \epsilon_{C-Pt}$), (b) Strong Gr-sub ($\epsilon_{GS} = 10\epsilon_{C-Pt}$, $\epsilon_{GT} = \epsilon_{C-Pt}$), (c) Strong Gr-tip ($\epsilon_{GS} = \epsilon_{C-Pt}$, $\epsilon_{GT} = 10\epsilon_{C-Pt}$), and (d) Strong Adhesion ($\epsilon_{GS} = 10\epsilon_{C-Pt}$, $\epsilon_{GT} = 10\epsilon_{C-Pt}$). Plots of force P vs. scaled penetration

depth h/R for graphene monolayer, bilayer, trilayer coatings on substrate are depicted in each subfigure. The insets show the snapshots of nanoindentation on monolayer and bilayer graphene-coated substrates. The schematic illustrations of tip-graphene-substrate adhesion are also presented for graphene monolayer cases, where the gray and red region indicates normal (ε_{C-Pt}) and strong adhesion ($10\varepsilon_{C-Pt}$), respectively.

3.2. Reduce adhesion strength by coating graphene layers

Recent studies [15, 16, 18] have revealed that coating graphene on substrate can mitigate adhesion between the substrate and the tip. To figure out the underlying mechanisms of graphene coating effects on nanoindentation, MS simulations are conducted on a Pt substrate with graphene layers. Moreover, a systematic analysis is performed to investigate the regulation of the elastic response of graphene-layers-covered substrate to nanoindentation based on the principles obtained for bare substrate.

Graphene monolayer coating: Therefore, we coat monolayer graphene onto substrate and simulate the indentation process of a Pt tip contacting an Pt substrate (inset, Fig. 2a). As the distance between the substrate and the tip increases due to the isolation of graphene, the adhesion on the tip is significantly reduced and the transferring of substrate atoms to the tip is also substantially constrained, appearing as an ideal method to eliminate adhesion. Specifically, the contact response of graphene-coated substrate is near the optimal contact behavior ($N = 1.44$ for black curve in Fig. 2a), in which both graphene-substrate and graphene-tip interaction are weak Pt-C adhesion.

Generally, graphene possesses weak adhesion to other materials, thus regulating contact behavior to the Hertz prediction. However, in some cases, graphene may unavoidably have strong adhesion with the tip or the substrate, such as the graphene-mica interaction [15, 36, 37] and interaction with oxidized graphene [38]. Therefore, the study on nanoscale contact when strong adhesion exists in either tip-graphene or graphene-substrate interaction is also urgently needed.

Fig. 2b-c illustrates two corresponding cases when strong adhesion is applied to graphene-substrate adhesion (Strong Gr-sub, $\varepsilon_{GS} = 10\varepsilon_{C-Pt}$, $\varepsilon_{GT} = \varepsilon_{C-Pt}$) and graphene-tip adhesion (Strong Gr-tip, $\varepsilon_{GS} = \varepsilon_{C-Pt}$, $\varepsilon_{GT} = 10\varepsilon_{C-Pt}$), respectively. It is demonstrated that the contact behavior is highly consistent with Hertz contact prediction in Strong Gr-sub case ($N = 1.48$ for black curve in Fig. 2b), whereas the graphene apparently loses its regulation effect in Gr-tip Adhesion case ($N = 1.31$ for black curve in Fig. 2c). Fig. 2b (inset) schematically illustrates that a strong graphene-substrate adhesion will not lead to force deviations because the tip force is not directly related to graphene-substrate interaction. Strong graphene-substrate adhesion can even contribute to the regulation of contact behavior by constraining graphene deformation and interfacial contact between graphene and tip, thus lessening graphene-tip adhesion [15, 16]. Consistently, it was demonstrated by Niu et al [39] and Zhou et al [40] that normal graphene-tip adhesion can be neglected when fitting FEM and MD simulations to the indentation experiment if strong graphene-substrate adhesion exists. As shown in Fig. 2c (inset), a proportion of graphene tightly adheres to the tip and the rest paved on the substrate significantly impacts the tip movement, thus deviating the loading force

to a large extent. For Gr-tip Adhesion case, graphene's high out-of-plane flexibility coupled with strong tip-graphene adhesion causes local puckering near the contact edge. The force-displacement curve for Strong Adhesion case ($\epsilon_{GS} = 10\epsilon_{C-pt}$, $\epsilon_{GT} = 10\epsilon_{C-pt}$) presents a strong deviation from the Hertz contact behavior ($N = 1.24$ for black curve in Fig. 2d), resulted from the observation that graphene firmly attaches both sides of interface and acts as intermediate for adhesion force (inset, Fig. 2d). It should also be given to the fact that force fluctuation does not appear in Gr-tip Adhesion case even if strong adhesion exists between the tip and the contact surface. This is attributed to high in-plane stiffness of graphene serving as an additional restriction to single atoms' transferring behavior. We conclude that graphene's effectiveness in modifying contact response also strongly relies on its unique properties, i.e., high in-plane stiffness [4] and low surface energy [5, 6]. That is also the reason why other coatings such as oxide layers lack this competence.

Multilayer graphene coatings: In order to further regulate adhesive contact behaviors for monolayer system in Strong Adhesion case, we increase the graphene coating into bilayer and trilayer (blue and red curves in Fig. 2). It has been reported that the friction of graphite and other lamellar materials increases with decreasing number of atomic layers [15, 16, 38]. Fig. 2d shows that the fitted exponent (1.40 for blue curve) for the load-displacement curve of bilayer coating of graphene is much closer to 1.50 than that of monolayer coating case (1.24 for black curve), but the small difference is due to the lateral constraint from the superficial graphene layer. The schematic indicates that the transmission of adhesion between tip and substrate is blocked due to the weak interlayer

interaction of graphene layers. As we further increase the graphene coating into trilayer, the fitted exponent for the load-displacement curve is also 1.40, same as that of bilayer coating. For strong tip-graphene and graphene-substrate interaction, the layer dependent regulation can be concluded that predominant effects can be aroused from monolayer to bilayer due to adhesion block by weak graphene interlayers interaction, but the same performance between bilayer and multilayer is the result of lateral constraint from graphene on the top. Note that this trend can be further supported by the experimental result of graphene coated nanoindentation from Suk et al [41], in which multilayer coating bears less adhesion energy and force gap. We then apply the multilayer coverage system into Gr-tip Adhesion case (Fig. 2c) and observe nearly identical contact response as that in strong adhesion case. This corroborates the abovementioned finding that graphene/substrate interaction cannot provide a substantial contribution to tip force when multilayer is applied.

Graphene coating on tip: Considering that, in aforesaid Gr-tip Adhesion case where a piece of graphene atoms tightly adheres to the tip and severely deviates the contact behavior, we naturally propose a method to coat graphene monolayer directly onto the tip rather than substrate [36, 42, 43]. Fig. 3 (inset) schematically elucidates the MS setup for graphene coated on the tip when adopting a strong graphene-tip adhesion and a normal graphene-substrate adhesion. From the load-displacement curve (blue colored) in Fig. 3c, we observe that the extracted fitting exponent $N = 1.39$, an apparent improvement compared to the model ($N = 1.31$) when graphene is paved on the substrate (black colored). The graphene coating on the tip serves as separation for tip-

substrate adhesion but does not affect the loading force regarding that in this case graphene can be viewed as a part of nanoindenter. The small deviation from 1.50 can also be rationalized by the influence from normal graphene-substrate adhesion because the adhering graphene can transmit adhesion force to the tip. However, this adhesive deviation can be substantially eliminated by applying monolayer graphene coating on each contact side as the interaction between graphene layers are very weak (see MD snapshots in Fig. 3c (Inset)). We also note that coating monolayer graphene directly onto the tip does not exert better effects for other three cases. However, further simulations demonstrate that coating graphene coverage on each side can also be positively influential for strong adhesion case regardless of the strength of graphene-substrate adhesion (Fig. 3d). The weak tip-graphene interaction does not hamper the modification though the wrinkles emerge at the margin of graphene due to geometrical mismatch between a sphere and a sheet (Fig. 3a-b). The full match of lowest part of graphene and tip is enough for the stage of elastic contact. That is, the contact region is too shallow to touch the graphene wrinkles as shown in Fig. 3a-b (inset, red circle).

From the abovementioned outcomes, under the circumstance of Gr-tip Adhesion or Gr-sub Adhesion, the most effectual way for monolayer graphene to diminish adhesion impacts is to apply graphene coverage to the strong-adhesion side, rendering segregation to adhesion effects. As confirmed by the simulation, under the circumstance of strong adhesion on both graphene-tip and graphene-substrate interaction, increasing graphene layers can be an ideal method for modifying contact behavior, whereas graphene on the top layer can confine tip movement to a large extent. Still, we reveal

that coating graphene on both contact sides can considerably improve the mitigation effect as the interlayer interaction among graphene is very weak. Furthermore, we need to mention that the original principle of this method is similar to that in the application of graphene-coated microsphere in superlubricity reported by Liu et al [36], in which adhesion segregation and weak interlayer forces are critical.

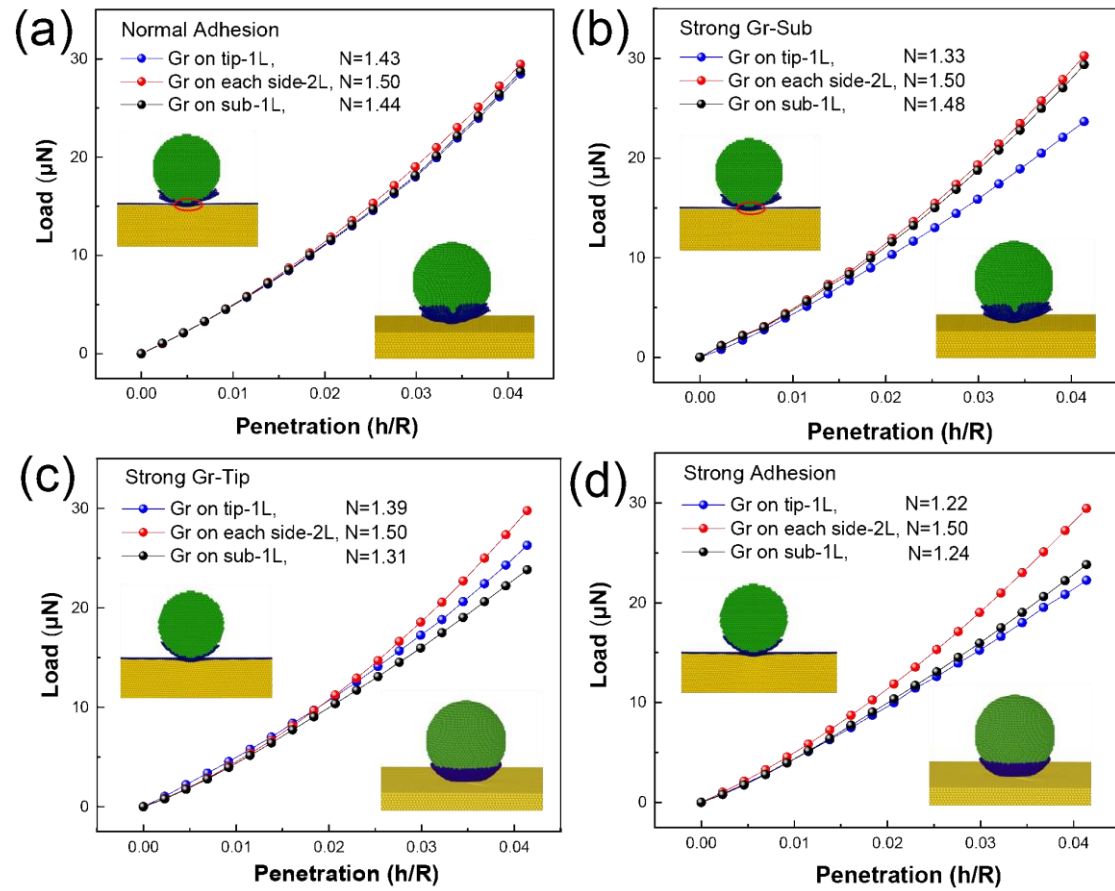


Figure 3. A novel morphology of paving graphene monolayer directly onto indenter tip for quasi adhesion-less contact for (a) Normal Adhesion ($\epsilon_{GS} = \epsilon_{C-pt}$, $\epsilon_{GT} = \epsilon_{C-pt}$), (b) Strong Gr-sub ($\epsilon_{GS} = 10\epsilon_{C-pt}$, $\epsilon_{GT} = \epsilon_{C-pt}$), (c) Strong Gr-tip ($\epsilon_{GS} = \epsilon_{C-pt}$, $\epsilon_{GT} = 10\epsilon_{C-pt}$), and (d) Strong Adhesion ($\epsilon_{GS} = 10\epsilon_{C-pt}$, $\epsilon_{GT} = 10\epsilon_{C-pt}$). Plots of force P vs. scaled penetration depth h/R for graphene monolayer coating on substrate, tip, or either side of the contacting interface are depicted in each subfigure. The insets show

the snapshots of nanoindentation with graphene-monolayer-coated tips on bare and graphene-monolayer-coated substrates.

3.3. Enhance substrate stiffness by applying pre-strain in graphene

As the facial contact stiffness of the substrate is associated with the flexibility of graphene [44], we apply equivalent and incremental biaxial in-plane strain and regulate their deformability to control the adhesive contact behavior. The purpose of strain engineering comes from our obtained results in section 3.2 that graphene appears low surface adhesion to other material and constraint to atom attachment by its inherent high in-plane stiffness. Meanwhile, with regard to the friction behavior, Zhang et al. have proposed that effective modulation has been achieved by tuning the flexibility of the graphene on substrate via in-plane straining [9]. Additionally, as has been stated in Fig. 1d, a substrate with ultrahigh stiffness can efficiently prevent interferences from adhesion of atoms in substrate. Therefore, a comprehensive study on the strain engineering to tune the prediction performance is worthwhile to do in the following parts.

In Fig. 4a, for the extreme conditions i.e., Strong Adhesion, compressive strain of -0.5% can noticeably enlarge the influence of adhesion on load deviations ($N = 0.97$ for blue curve) but tensile strain up to 4.5% can completely eliminate adhesion effects ($N = 1.50$ for red curve). As illustrated in top panels of Fig. 4b, compressive strain renders a more flexible configuration and results in a more intimate contact (left panel), whereas a tensile strain increases the facial stiffness, producing a less-pinned graphene-tip interface (right panel). Atoms on graphene coating that provide repulsive forces prevent

tip penetration, while adhesion is related to atoms on graphene coating that provide adhesive forces to the tip. Therefore, we calculate the normal atomic stress (σ_{zz}) distribution for graphene monolayer at the same depth-radius ratio $h/R = 0.1$. The stress distribution of graphene monolayer with various strain are shown in the bottom panel of Fig. 4b, indicating that the number of adhesive atoms (red, $\sigma_{zz} > 0.1GPa$) decreases with increasing pre-strain, whereas the number of repulsive atoms (blue, $\sigma_{zz} < -0.1GPa$) almost keeps unchanged on the same level. Therefore, the adhesion can be significantly mitigated by applying pre-strain in graphene before nanoindentation. For Normal Adhesion, the load-displacement curves and atomic configurations in Fig. 4c-d show exactly the same trend with Fig. 4a-b, indicating that applying tensile pre-strain in graphene coating on substrate is an effective method to modulate elastic behavior of nanoindentation.

To quantitatively describe the effect of in-plane strain during contact, the fitting exponent N versus biaxial strain curve is shown in Fig. 5. The fitting exponent of load-displacement curves increase monotonically with incremental tensile strain and gradually levels off at high strain, indicating the gradual reduction and eventual elimination of adhesion interference. This outcome is understandable as strain engineering in graphene would change the out-of-plane flexibility and adjust the adhering behavior of graphene atoms to the tip, thereby affecting adhesion strength and contact quality. Therefore, by tuning the in-plane strain of graphene, we demonstrate that the surface adhesion of graphene-substrate system to the tip can be well regulated by altering the contact stiffness and atomic-scale adhering quality. This conclusion

gives the very example, where the atomic-scale contact behaviors can be directly regulated via mechanical deformation.

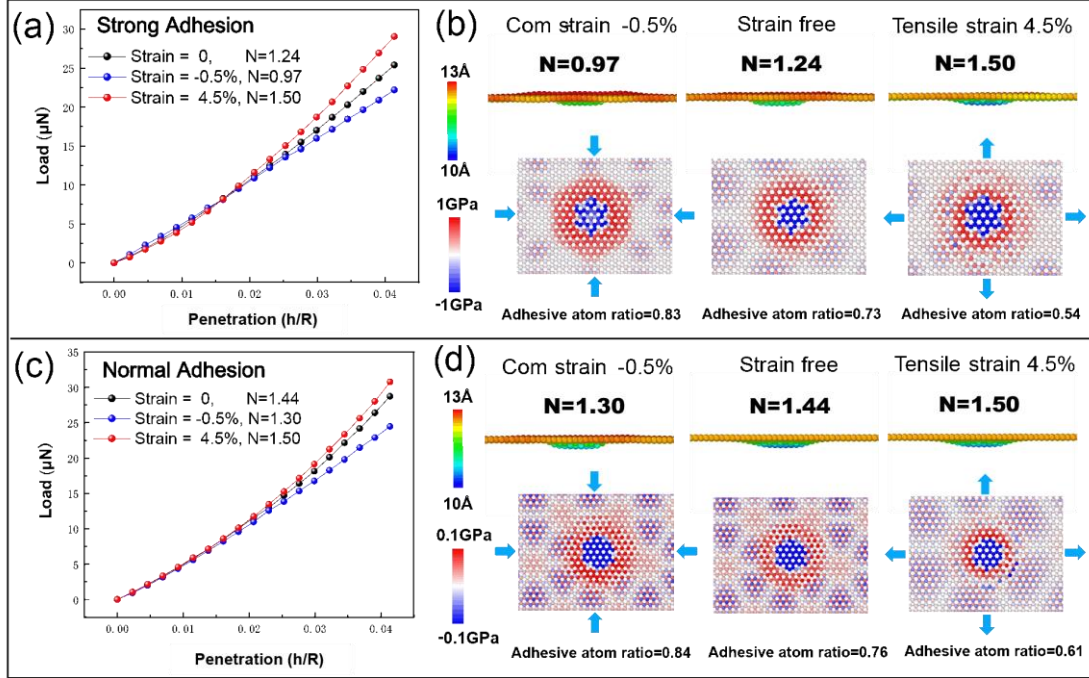


Figure 4. Modulation of contact behavior on graphene-monolayer-coated Pt substrate with biaxial in-plane pre-strains for (a-b) Strong Adhesion ($\varepsilon_{GS} = 10\varepsilon_{C-Pt}$, $\varepsilon_{GT} = 10\varepsilon_{C-Pt}$) and (c-d) Normal Adhesion ($\varepsilon_{GS} = \varepsilon_{C-Pt}$, $\varepsilon_{GT} = \varepsilon_{C-Pt}$). (a, c) Plots of force P vs. scaled penetration depth h/R for graphene monolayer with -0.5%, 0, and +4.5% biaxial pre-strain. (b, d) Side (top panel) and top (bottom panel) views for the graphene monolayer with different pre-strain when the penetration depth h/R equals 0.1. The color for each atom represents the out-of-plane displacement (u_z) and atomic stress component (σ_{zz}), respectively. The ratio of adhesive atoms is calculated as based on the identification of repulsive atoms ($\sigma_{zz} < 0.1\sigma_{zz}^{min}$) and adhesive atoms ($\sigma_{zz} > 0.1\sigma_{zz}^{max}$), where $(\sigma_{zz}^{min}, \sigma_{zz}^{max})$ are $(-1GPa, 1GPa)$ and $(-0.1GPa, 0.1GPa)$ for (b) Strong Adhesion and (d) Normal Adhesion, respectively.

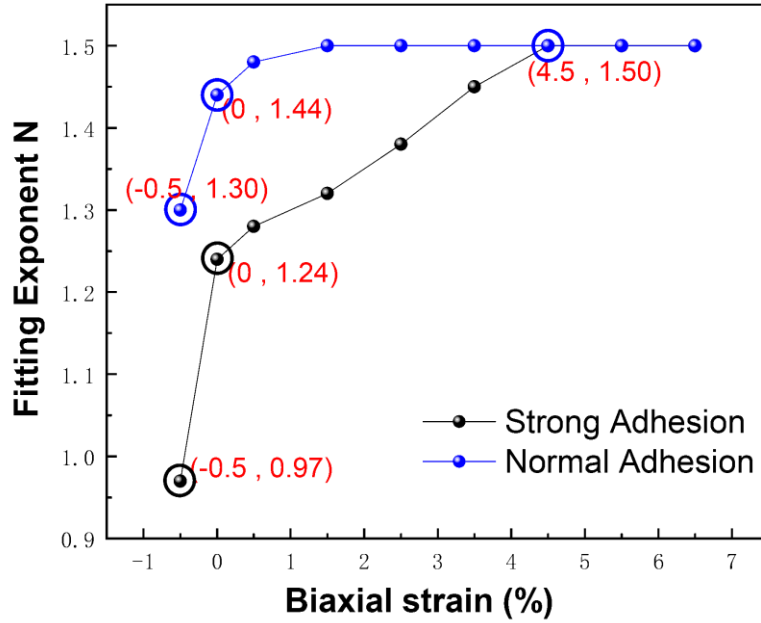


Figure 5. Exponent N by fitting $P = (4E^*R^2/3) (h/R)^N$ versus biaxial pre-strain of the graphene monolayer coating for Strong Adhesion ($\varepsilon_{GS} = 10\varepsilon_{C-Pt}$, $\varepsilon_{GT} = 10\varepsilon_{C-Pt}$) and Normal Adhesion ($\varepsilon_{GS} = \varepsilon_{C-Pt}$, $\varepsilon_{GT} = \varepsilon_{C-Pt}$). The black and blue open circles correspond to the MS simulations shown in Fig. 4a and 4c, respectively.

3.4. Size effect on nanoscale adhesive contact

As represented in Fig. 6a, to explore the effect of tip size, two indenter tips with different sizes (radii of 5nm and 20nm) are produced to indent the graphene-monolayer-covered Pt substrate. To carry out a thorough comparison, 3 typical tip-graphene interactions are adopted here, namely, 1) Purely repulsive potential, 2) Normal Adhesion, and 3) Strong Adhesion. The values of the exponent N calculating from the fittings are provided in Fig. 6b-c, showing that indentations with large indenter size exhibit a closer agreement with Hertz law. As illustrated in Fig. 1c (inset), the atoms

providing adhesive forces to the tip (red) are only located at the margin of the contact interface, while the atoms preventing tip penetration (blue) are located on the contact surface. Hence, for the same depth-radius ratio h/R , we estimate that the number of adhesive atoms of graphene is proportional to the tip size, $N_a \propto R$. As a counterpart, based on the Hertz contact theory, the number of repulsive atoms of graphene, i.e. the contact area, is estimated to be proportional to the square of tip size, $N_r \propto R^2$. We conclude that the proportion of adhesive atoms can be inversely proportional to the tip size, $N_a/N_r \propto 1/R$, which leads to the significant influence of adhesion for smaller tip size. To further quantify the proportion of adhesive atoms for different tip sizes, we calculate the normal atomic stress (σ_{zz}) distribution for the graphene monolayer at the same depth-radius ratio $h/R = 0.2$. Fig. 6b-d shows the stress distribution of graphene monolayer for 5nm and 20nm tips with 3 typical adhesion cases, respectively. It can be seen clearly from Fig. 6b that a purely repulsive interaction could result in entirely repulsive forces of graphene atoms in contact, whereas the proportion of atoms with adhesive forces can gradually increase with increasing adhesion as shown in Fig. 6c and 6d. The atoms with positive stress (red) provide adhesive force to indentation, whereas those with negative stress (blue) hinder tip penetration. Here we need to point out that the periodic stress distribution out of the contact area manifests the impacts of moiré pattern formed between graphene and supporting crystalline substrate [45, 46]. In order for a more quantitative description of the contact property, proportions of atoms with adhesive forces to the whole atoms in contact (adhesive atom ratio) and contact area providing repulsive forces (repulsive contact area) are calculated for each

model. From Fig. 6b-d, we could verify our previous theoretical estimation that a larger tip possesses less proportion of adhesive atoms during contact. Meanwhile, for tips with a uniform size, the repulsive contact area is steady regardless of adhesion strength. For particular adhesion conditions, the ratio of repulsive contact area between tips with two different sizes are respectively, 12.31, 13.76, 14.60, close to above theoretical value (=16). Our conclusion corroborates with results of others calculated from FEA method [47]. It is worth noting that the tip size effect is more significant for strong adhesion than the normal adhesion, and the contact behavior of purely repulsive case is independent on the tip size, shown in Fig. 6b-d. Aside from the fundamental mechanism, the tip-size effect also emphasizes the significance of a better insight into the adhesive contact behavior especially at the nanoscale, that is, contact at this scale will largely deviate from the traditional elastic model owing to apparent adhesion.

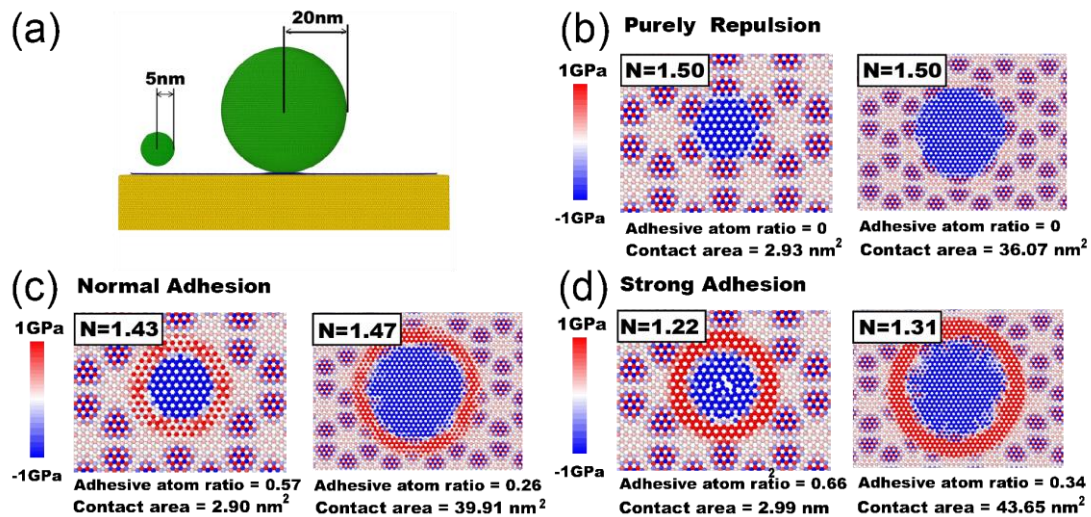


Figure 6. The effect of tip size on adhesive contact behavior. (a) Schematic illustration of nanoindentation on a graphene-monolayer-covered Pt substrate with indenters of radii of $R = 5$ and 20 nm. (b-d) Atomic stress distribution for the graphene

monolayer on Pt substrates at the contact interface as the penetration depth $h/R = 0.2$ for 5 nm (left) and 20 nm (right) tips. The color for each atom represents the atomic stress (σ_{zz}) component. The ratio of adhesive atoms is calculated based on the identification of repulsive atoms ($\sigma_{zz} < -0.1GPa$) and adhesive atoms ($\sigma_{zz} > 0.1GPa$). Here three typical adhesions are applied as (b) Purely repulsive interaction, (c) Normal Adhesion ($\varepsilon_{GS} = \varepsilon_{C-Pt}, \varepsilon_{GT} = \varepsilon_{C-Pt}$), and (d) Strong Adhesion ($\varepsilon_{GS} = 10\varepsilon_{C-Pt}, \varepsilon_{GT} = 10\varepsilon_{C-Pt}$). The corresponding exponents N are extracted by fitting $P = (4E^*R^2/3) (h/R)^N$ to load-displacement curves from MS simulations.

4. Conclusions

In conclusion, nanoindentation simulations show that the elastic contact behavior of metallic substrate exhibits a near ideal Hertzian contact, achieved by coating graphene layers on either side of the contact interface. This regulation effect can be explained by graphene's high in-plane strength and low surface energy, which originates from the modification of the interaction forces between the tip and the indented surface. For bare substrate, the effect of adhesion on nanoindentation can be significantly mitigated by reducing the amplitude and range of atomic interaction between tip and substrate, or enhancing substrate stiffness. Aforesaid principle shows that the elastic contact behavior for specific indenter/substrate interaction can be regulated by increasing the coated graphene layers due to the weak interlayer interaction between layers. Furthermore, the elastic contact behavior is more near the Hertz prediction using larger size indenter or applying pre-strains to graphene layers. Our study confirms some

related experimental results reported by other researchers and provides a theoretical guidance on designing adhesion-less coatings for the AFM probes and MEMS/NEMS systems.

Credit authorship contribution statement

Yongchao Chen: Methodology, Investigation, Formal analysis, Writing-original draft.

Zhizi Guan: Investigation, Formal analysis, Writing-review & editing. Yongtao Yao:

Writing - review & editing, Supervision. Hailong Wang: Conceptualization, Formal analysis, Writing - review & editing, Supervision.

Declaration of competing interest

The authors declare that they have no known competing financial interests or personal relationships that could have appeared to influence the work reported in this paper.

Acknowledgments

We acknowledge support from Science Foundation of the National Key Laboratory of Science and Technology on Advanced Composites in Special Environments and the fundamental Research Funds for the Central Universities (grant no. WK2090050042).

References:

- [1] Novoselov, K. S. Electric Field Effect in Atomically Thin Carbon Films. *SCIENCE*. 2004;306(5696):666-9.
- [2] Zhang S, Ma T, Erdemir A, Li Q. Tribology of two-dimensional materials: From mechanisms to modulating strategies. *MATER TODAY*. 2019 2019-01-01;26:67-86.
- [3] Berman D, Erdemir A, Sumant AV. Graphene as a protective coating and superior lubricant for electrical contacts. *APPL PHYS LETT*. 2014;105(23):231907.
- [4] Lee C, Wei X, Kysar JW, Hone J. Measurement of the Elastic Properties and Intrinsic Strength of Monolayer Graphene. *SCIENCE*. 2008;321(5887):385-8.
- [5] Wang S, Zhang Y, Abidi N, Cabrales L. Wettability and Surface Free Energy of Graphene Films. *LANGMUIR*. 2009 2009-09-15;25(18):11078-81.
- [6] Kim KS, Lee H, Lee C, Lee S, Jang H, Ahn J, et al. Chemical Vapor Deposition-Grown Graphene: The Thinnest Solid Lubricant. *ACS NANO*. 2011;5(6):5107-14.
- [7] Nilsson L, Andersen M, Balog R, Lægsgaard E, Hofmann P, Besenbacher F, et al. Graphene

Coatings: Probing the Limits of the One Atom Thick Protection Layer. ACS NANO. 2012 2012-11-27;6(11):10258-66.

[8] Li S, Li Q, Carpick RW, Gumbsch P, Liu XZ, Ding X, et al. The evolving quality of frictional contact with graphene. NATURE. 2016;539(7630):541-5.

[9] Zhang S, Hou Y, Li S, Liu L, Zhang Z, Feng X, et al. Tuning friction to a superlubric state via in-plane straining. Proceedings of the National Academy of Sciences. 2019 2019-12-03;116(49):24452-6.

[10] Vasić B, Matković A, Ralević U, Belić M, Gajić R. Nanoscale wear of graphene and wear protection by graphene. CARBON. 2017 2017-01-01;120:137-44.

[11] Klemenz A, Gola A, Moseler M, Pastewka L. Contact mechanics of graphene-covered metal surfaces. APPL PHYS LETT. 2018 2018-02-05;112(6):61601.

[12] Klemenz A, Pastewka L, Balakrishna SG, Caron A, Bennewitz R, Moseler M. Atomic Scale Mechanisms of Friction Reduction and Wear Protection by Graphene. NANO LETT. 2014 2014-12-10;14(12):7145-52.

[13] Xu Q, Li X, Zhang J, Hu Y, Wang H, Ma T. Suppressing Nanoscale Wear by Graphene/Graphene Interfacial Contact Architecture: A Molecular Dynamics Study. ACS APPL MATER INTER. 2017 2017-11-22;9(46):40959-68.

[14] Peng W, Sun K, Abdullah R, Zhang M, Chen J, Shi J. Strengthening mechanisms of graphene coatings on Cu film under nanoindentation: A molecular dynamics simulation. Applied Surface Science. 2019;487(SEP.1):22-31.

[15] Li Q, Lee C, Carpick RW, Hone J. Substrate effect on thickness-dependent friction on graphene. physica status solidi (b). 2010;247(11-12):2909-14.

[16] Lee C, Li Q, Kalb W, Liu XZ, Berger H, Carpick RW, et al. Frictional characteristics of atomically thin sheets. SCIENCE. 2010 2010-04-02;328(5974):76-80.

[17] Park S, Kim Y, Ruoff RS, Kim J. Incipient plasticity and fully plastic contact behavior of copper coated with a graphene layer. APL MATER. 2019;7(3):31106.

[18] Hammad M, Adjizian JJ, Sacré CH, Huet B, Charlier JC, Raskin JP, et al. Adhesionless and near-ideal contact behavior of graphene on Cu thin film. CARBON. 2017 2017-01-01;122:446-50.

[19] Johnson KL, Kendall K, Roberts ADA. Surface Energy and the Contact of Elastic Solids. Proc.r.soc.lond.a. 1971;324(1558):301-13.

[20] Galanov BA. Models of adhesive contact between rough elastic solids. INT J MECH SCI. 2011;53(11):968-77.

[21] Song J, Srolovitz DJ. Adhesion effects in material transfer in mechanical contacts. ACTA MATER. 2006 2006-01-01;54(19):5305-12.

[22] Milne ZB, Bernal RA, Carpick RW. Sliding History-Dependent Adhesion of Nanoscale Silicon Contacts Revealed by in Situ Transmission Electron Microscopy. LANGMUIR. 2019 2019-12-03;35(48):15628-38.

[23] Milne Z, Schall JD, Jacobs TDB, Harrison JA, Carpick RW. Covalent Bonding and Atomic-Level Plasticity Increase Adhesion in Silicon-Diamond Nanocontacts. ACS APPL MATER INTER. 2019 2019-01-01;11(43):40734-48.

[24] Xu S, Wan Q, Sha Z, Liu Z. Molecular dynamics simulations of nano-indentation and wear of the γ Ti-Al alloy. COMP MATER SCI. 2015;110:247-53.

[25] He X, Bai Q, Shen R. Atomistic perspective of how graphene protects metal substrate from surface damage in rough contacts. CARBON. 2018 2018-01-01;130:672-9.

[26] Daneshmand M, Mansour RR. RF MEMS Satellite Switch Matrices. IEEE MICROW MAG.

2011;12(5):92-109.

[27] Kwon H, Choi D, Park J, Lee H, Park Y, Kim Y, et al. Contact materials and reliability for high power RF-MEMS switches.; 2007 2007-01-01: IEEE; 2007. p. 231-4.

[28] Hyman D, Mehregany M. Contact physics of gold microcontacts for MEMS switches. *Components & Packaging Technologies IEEE Transactions on*. 1999;22(3):357-64.

[29] Plimpton S. Fast Parallel Algorithms for Short-Range Molecular Dynamics. *J COMPUT PHYS*. 1995 1995-01-01;117(1):1-19.

[30] Zhou X, Johnson R, Wadley H. Misfit-energy-increasing dislocations in vapor-deposited CoFe/NiFe multilayers. *PHYS REV B*. 2004;69(14):144113.

[31] Brenner DW, Shenderova OA, Harrison JA, Stuart SJ, Ni B, Sinnott SB. A second-generation reactive empirical bond order (REBO) potential energy expression for hydrocarbons. *Journal of Physics Condensed Matter*. 2002;14(4):783-802.

[32] Pastewka L, Pou P, Pérez R, Gumbsch P, Moseler M. Describing bond-breaking processes by reactive potentials: Importance of an environment-dependent interaction range. *Physical review*. 2008;78(16):53-6.

[33] Dodson BW. Development of a many-body Tersoff-type potential for silicon. *PHYS REV B*. 1987 1987-02-15;35(6):2795-8.

[34] Mendeleev MI, Kramer MJ, Becker CA, Asta M. Analysis of semi-empirical interatomic potentials appropriate for simulation of crystalline and liquid Al and Cu. *PHILOS MAG*. 2008 2008-04-21;88(12):1723-50.

[35] Peeters FM, Neek-Amal M. Nanoindentation of a circular sheet of bilayer graphene. *PHYS REV B*. 2010 2010-06-11;81(23):235421.

[36] Liu SW, Wang HP, Xu Q, Ma TB, Yu G, Zhang C, et al. Robust microscale superlubricity under high contact pressure enabled by graphene-coated microsphere. *NAT COMMUN*. 2017 2017-02-14;8:14029.

[37] Zhang J, Chen X, Xu Q, Ma T, Hu Y, Wang H, et al. Effects of grain boundary on wear of graphene at the nanoscale: A molecular dynamics study. *CARBON*. 2019;143:578-86.

[38] Deng Z, Smolyanitsky A, Li Q, Feng X, Cannara RJ. Adhesion-dependent negative friction coefficient on chemically modified graphite at the nanoscale. *NAT MATER*. 2012;11(12):1032-7.

[39] Niu T, Cao G, Xiong C. Indentation Behavior of the Stiffest Membrane Mounted on a Very Compliant Substrate: Graphene on PDMS. *INT J SOLIDS STRUCT*. 2017:S2144540944.

[40] Zhou L, Wang Y, Cao G. Estimating the elastic properties of few-layer graphene from the free-standing indentation response. *J Phys Condens Matter*. 2013;25(47):475301.

[41] Suk JW, Na SR, Stromberg RJ, Stauffer D, Lee J, Ruoff RS, et al. Probing the adhesion interactions of graphene on silicon oxide by nanoindentation. *CARBON*. 2016;103:63-72.

[42] Hui F, Vajha P, Shi Y, Ji Y, Duan H, Padovani A, et al. Moving graphene devices from lab to market: advanced graphene-coated nanoprobe. *NANOSCALE*. 2016 2016-01-01;8(16):8466-73.

[43] Martin-Olmos C, Rasool HI, Weiller BH, Gimzewski JK. Graphene MEMS: AFM Probe Performance Improvement. *ACS NANO*. 2013 2013-05-28;7(5):4164-70.

[44] Kitt AL, Qi Z, Remi S, Park HS, Goldberg BB. How graphene slides: measurement and theory of strain-dependent frictional forces between graphene and SiO₂. *NANO LETT*. 2013;13(6).

[45] Liu J, Zhang S, Li Q, Feng X, Di Z, Ye C, et al. Lateral force modulation by moiré superlattice structure: Surfing on periodically undulated graphene sheets. *CARBON*. 2017 2017-01-01;125:76-83.

[46] Chan N, Balakrishna SG, Klemenz A, Moseler M, Egberts P, Bennewitz R. Contrast in nanoscale

friction between rotational domains of graphene on Pt(111). CARBON. 2017 2017-01-01;113:132-8.

[47] Zhang X, Zhang X, Wen S. Finite Element Modeling of the Nano-scale Adhesive Contact and the Geometry-based Pull-off Force. TRIBOL LETT. 2011;41(1):65-72.